POWDER DIFFRACTION

CAMBRIDGE UNIVERSITY PRESS

X-ray powder diffraction analysis of two new magnesium selenate hydrates, $MgSeO_4 \cdot 9H_2O$ and $MgSeO_4 \cdot 11H_2O$

Journal:	*Powder Diffraction*
Manuscript ID:	PD-TA-2014-0049.R4
Manuscript Type:	Technical Article
Date Submitted by the Author:	n/a
Complete List of Authors:	Fortes, Andrew; Department of Earth Sciences, University College London - Gower Street - London - WC1E 6BT
Keywords:	magnesium selenate, enneahydrate, undecahydrate, meridianiite
Note: The following files were submitted by the author for peer review, but cannot be converted to PDF. You must view these files (e.g. movies) online.	
MgSeO4_9H2O.cif	

X-ray powder diffraction analysis of two new magnesium selenate hydrates, $MgSeO_4 \cdot 9H_2O$ and $MgSeO_4 \cdot 11H_2O$

A. Dominic Fortes[1,2,a)]

[1]*Department of Earth Sciences, University College London, Gower Street, London WC1E 6BT, U.K.*

[2]D*epartment of Earth and Planetary Sciences, Birkbeck, University of London, Malet Street, London WC1E 7HX*

Abstract

Several hitherto unknown hydrates of magnesium selenate have been formed by quenching aqueous solutions of $MgSeO_4$ in liquid nitrogen. $MgSeO_4 \cdot 11H_2O$ is apparently isostructural with the mineral meridianiite ($MgSO_4 \cdot 11H_2O$), being triclinic, $P\bar{1}$, $Z = 2$, with unit-cell parameters $a = 6.77900(8)$ Å, $b = 6.96516(9)$ Å, $c = 17.4934(2)$ Å, $\alpha = 87.713(1)°$, $\beta = 89.222(1)°$, $\gamma = 63.121(1)°$, and $V = 736.15(1)$ Å^3 at −25 °C. $MgSeO_4 \cdot 9H_2O$ represents a new hydration state in the $MgSeO_4$–H_2O system; it is monoclinic, space-group $P2_1/c$, $Z = 4$, with unit-cell parameters $a = 7.27024(6)$ Å, $b = 10.51094(9)$ Å, $c = 17.4030(2)$ Å, $\beta = 109.447(1)°$, and $V = 1254.02(1)$ Å^3 at −22 °C. The heavy-atom structure of $MgSeO_4 \cdot 9H_2O$ has been determined by direct-space methods from X-ray powder diffraction data and consists of isolated $Mg(H_2O)_6^{2+}$ octahedra and SeO_4^{2-} tetrahedra linked by hydrogen bonds. The remaining three water molecules occupy the space between the polyhedral ions, contributing to the H-bonded network, which comprises 4–, 5– and 6–membered rings. A third phase has been observed to crystallise prior to the 11-hydrate upon warming of liquid-nitrogen-quenched glass, but this transforms rapidly to the meridianiite-structured 11-hydrate and the identity of this phase is unclear.

Keywords: magnesium selenate, enneahydrate, undecahydrate, meridianiite

[a)]Author to whom correspondence should be addressed. Electronic mail andrew.fortes@ucl.ac.uk

I. INTRODUCTION

In recent years I have been studying the occurrence of crystalline hydrates with the general formula $M^{2+}XO_4 \cdot nH_2O$ that form at low temperatures (at or below the freezing point of ice) with n in the range 7 to 11. This work is motivated principally by an interest in 'planetary' cryohydrates such as $MgSO_4 \cdot 11H_2O$. This substance occurs naturally on Earth as the mineral meridianiite, being found in glacial and periglacial environments (Genceli *et al*., 2009) and in a limited number of $MgSO_4$–rich hypersaline lakes during the winter months (Peterson *et al*., 2007). However, meridianiite may occur globally on Mars, forming a substantial reservoir of bound water in the near-surface regolith (Peterson & Wang, 2006), and it may also be an important rock-forming mineral inside the icy Galilean moons of Jupiter (Kargel, 1991).

In a series of papers, my colleagues and I reported the results of work to form structural analogues of $MgSO_4 \cdot 11H_2O$ in which the cation was replaced by Mn^{2+}, Fe^{2+}, Co^{2+}, Ni^{2+}, Cu^{2+} or Zn^{2+} (Fortes *et al*., 2012a, 2012b) and the oxyanion was replaced by CrO_4^{2-} (Fortes & Wood, 2012: Fortes *et al*., 2013). These efforts provide information on the response of the structure to chemically-induced 'internal' stress that are complementary to other means of generating strain in the crystal, such as variable temperature and pressure (*cf*., Fortes *et al.,* 2008, 2009, 2012c). It was determined that only Mg^{2+} formed an end-member 11-hydrate, although there were some examples of considerable substitution for Mg^{2+} in the 11-hydrate structure (> 50 mol. % by Co^{2+} and Mn^{2+} for example). Conversely, it was found that a complete solid solution is possible between 11-hydrate end-members of $MgSO_4$ and $MgCrO_4$. The most surprising discovery was of a new hydration state: crystals containing nine water molecules per formula unit, were obtained from aqueous solutions of $(Mg,Ni)SO_4$, $(Mg,Zn)SO_4$, $(Mg,Fe)SO_4$ and $(Mg,Cu)SO_4$ by rapid quenching in liquid nitrogen. In subsequent work it has proven possible to obtain the end-member enneahydrates $MgSO_4 \cdot 9H_2O$ and $MgSO_4 \cdot 9D_2O$ (Fortes, 2014).

Given recent interest in highly hydrated sodium sulfate selenates (Weil and Bonneau, 2014), which includes the discovery of a new hydration state, $Na_2SeO_4 \cdot {}^{15}/_{2}H_2O$ (Kamburov *et al*., 2014), it seems useful to extend these earlier studies of ion substitution to include Mg-selenate hydrates.

The solid-liquid phase equilibria in the $MgSeO_4$—H_2O binary system have been the subject of some disagreement, there being significant differences between the observations of Meyer & Aulich (1928) and those of Klein (1940). In neither instance was the behaviour below the freezing point of ice characterised, the solubility curves and eutectic being found by extrapolation. Up until now, the highest hydrate found in this system, and the phase believed to be in equilibrium at the eutectic (−7 °C), was the heptahydrate, $MgSeO_4 \cdot 7H_2O$. Consequently, an important aspect of this work was to prepare and characterise the heptahydrate, since no crystallographic data on this phase had been reported previously. A single-crystal neutron diffraction experiment was undertaken and the results are reported elsewhere (Fortes & Gutmann, 2014). In brief, $MgSeO_4 \cdot 7H_2O$ is orthorhombic, space-group $P2_12_12_1$, and is isostructural with the sulfate analogue (epsomite).

A highly productive method to survey the occurrence of both stable and metastable low-temperature hydrates is flash-freezing of aqueous solutions in liquid nitrogen. The work reported here employs this technique, as outlined in the following section.

II. EXPERIMENTAL

A. Sample preparation

An aqueous solution of magnesium selenate was prepared as follows: commercially available aqueous H_2SeO_4 (Sigma-Aldrich 481513, 40 wt. %) was diluted to 25 wt. % H_2SeO_4 (1.72 M) with distilled water (Alfa-Aesar, ACS Reagent Grade, 36645), which was then heated to ~ 70 °C. To this liquid was added a molar excess of powdered MgO (Sigma Aldrich 342793, >99 % trace metals basis, -

325 mesh); specifically, 6 g of MgO was added to 100 g of hot 1.72 M solution. Since this synthesis, unlike the reaction with basic Mg-carbonate, is quiescent its progress was followed with a Tecpel hand-held pH meter. Once the pH of the solution stabilised at 8.80, the supernatant liquid was decanted, triply filtered and left to stand. Evaporation in the open air led to precipitation of cm-sized crystals of $MgSeO_4 \cdot 6H_2O$ from solution. After a further round of re-crystallisation from distilled water the phase purity of the hexahydrate was verified by X-ray powder diffraction. Finally, crystalline Mg-selenate hexahydrate was dissolved in distilled water at concentrations from 25–40 wt. % $MgSeO_4$. Quench specimens were prepared in one of two ways; firstly, ~ 1 cm^3 of liquid was poured directly into ~ 30 cm^3 of liquid nitrogen held in a steel cryomortar (∅ = 60 mm, depth = 20 mm), freezing rapidly to form a large white solid lump with regions of transparent (presumably glassy) material in its interior. Secondly, a pipette, filled with aqueous $MgSeO_4$ solution was used to deposit droplets into a pool of liquid nitrogen, which formed spherules from 2–6 mm in diameter. Observations made previously on nitrogen-quenched $MgSO_4$ and $MgCrO_4$ solution led me to believe that differences in cooling rates between the larger globules and the smaller spherules might influence the local structure of the solute-rich glass produced by quenching and thereby alter the phase produced on annealing. Once frozen, both the globules and the spherules were pulverized and ground to a powder with a nitrogen-cooled steel pestle.

B. X-ray powder diffraction

X-ray powder diffraction data were collected on a PANanalytical X'Pert Pro multipurpose powder diffractometer (using germanium monochromated Co $K\alpha_1$ radiation, λ = 1.788996 Å, and an X'Celerator multi-strip detector) equipped with a thermoelectrically cooled cold stage (Wood *et al.*, 2012). This portable cold stage was held in a plastic box filled with dry-ice pellets whilst the powder specimen was prepared and loaded, thereby chilling it to around −80 °C. The samples were transferred to the cold stage with a nitrogen-cooled spoon and the surface was flattened with the flat section of a spoon handle,

forming a top-loaded pressed powder specimen. The cover and fan assembly of the cold stage were screwed into place with the body of the stage still embedded in dry ice. In practice, once the power supply to the Peltier element and cooling fans is connected and the stage is screwed onto the diffractometer mounting bracket, the sample temperature rises to −30 °C in under ten minutes, eventually equilibrating at −20 to −25 °C (depending on the ambient temperature in the XRD enclosure) within twenty minutes. Thereafter, the sample temperature remains stable within a degree for many hours. Typically, a 20-minute scan in 2θ is carried out during the equilibration period; as described below, this often affords the opportunity to observe transient low-temperature metastable phases (even if they transform during the measurement) that could not be detected otherwise.

Data were collected with variable divergence and receiving slits, converted to fixed-slit geometry with the proprietary X'Pert Pro 'HighScore Plus' software package and then exported in an appropriate format for analysis in the GSAS/Expgui package (Larsen and Von Dreele, 2000; Toby, 2001).

III. RESULTS

As expected, the quenching of aqueous $MgSeO_4$ into either large globules or small spherules produced different results. Figure 1 gives examples of powder diffraction data collected from specimens formed by the two techniques. The globules of aqueous $MgSeO_4$ produced the diffraction pattern shown at the bottom of Figure 1 during the 20-minute period of thermal equilibration, which is dominated by Bragg peaks from water ice (phase Ih) and a number of less intense peaks from a crystalline hydrate of $MgSeO_4$. During this brief measurement, the $MgSeO_4$–hydrate underwent a transformation to another phase, which then persisted at −25 °C for the duration of the subsequent measurement (middle pattern in Figure 1). The spherules, on the other hand, produced the diffraction pattern shown at the top of Figure 1, both during the equilibration phase and thereafter, proving to be remarkably stable even when warmed above 0 °C.

A. Meridianiite-structured $MgSeO_4$ 11-hydrate

Neither the top or bottom diffraction patterns shown in Figure 1 resembled any phase seen previously. However, the middle pattern closely resembles (both in terms of peak positions and intensities) the powder diffraction patterns of $MgSO_4 \cdot 11H_2O$ and $MgCrO_4 \cdot 11H_2O$ reported previously (see figures in Wood *et al*., 2012, and Fortes & Wood, 2012). Since this structure is substantially strained with respect to the analogous sulfate and chomate, it proved necessary to index the Bragg peaks using DICVOL06 (Boultif & Louër, 2004); the unit-cell was subsequently refined by the LeBail method to yield the unit-cell parameters listed in Table I. Both the volume and axial strains caused by replacement of SO_4^{2-} with SeO_4^{2-} are roughly similar to those found on replacement with CrO_4^{2-}, which should not be surprising since the Se–O and Cr–O bond lengths are virtually identical (1.64 Å compared to 1.47 Å for S–O). The chemically-induced strains caused by oxyanion exchange in the selenate and chromate analogues of the undecahydrate are highly anisotropic, the most strained direction being along the *b*-axis. This direction is perpendicular to the corrugated sheets in the $MgSO_4 \cdot 11H_2O$ structure, which are connected by a mixture of single and bifurcated hydrogen bonds (Fortes *et al.,* 2008, 2013). Since the data collection for these specimens extended only to 90° 2θ (1.26 Å resolution) and the hydrate represented a little under 40 wt. % of the sample, the remainder being water ice, Rietveld refinement of the structure proved possible only with extremely rigid bond-distance and bond-angle restraints and fixed isotropic displacement parameters. Whilst this demonstrated to my satisfaction that there are no significant differences between the heavy atom structures of $MgSeO_4 \cdot 11H_2O$ and its chromate analogue, the accuracy of the atomic coordinates given in Table II is likely to be considerably poorer than for the previously reported $MgCrO_4 \cdot 11H_2O$ and $MgSO_4 \cdot 11H_2O$ structures (Fortes *et al.,* 2008: Fortes & Wood, 2012: Fortes *et al*., 2013).

B. Unknown $MgSeO_4$ hydrate

The phase that appears prior to the newly-discovered $MgSeO_4 \cdot 11H_2O$ described above has proven difficult to characterize, since the operation of the Peltier cold stage allows only a brief observation of its powder diffraction pattern whilst it is in the process of transforming to the more stable 11-hydrate, and there is a large variation in temperature during the scan. The most intense Bragg peaks from the meridianiite-structure 11-hydrate, which form a 'clump' around 20.70 – 20.85° 2θ, are marked with an asterisk in Figure 1 and the prevalence of unindexed peaks increases up to the point where the dataset has been truncated. An indexing of the least ambiguous Bragg peaks has been obtained using DICVOL06, but confidence in the accuracy of this result is impossible to determine at present. The indexing yielded a triclinic solution with unit-cell dimensions a = 7.449(5) Å, b = 6.003(4) Å, c = 8.651(6) Å, α = 76.65(8)°, β = 94.79(5)°, γ = 103.86(5)°, and V = 365.30 Å^3, the figures of merit M(10) = 55.8 and F(10) = 49.1 (0.0089, 23) (De Wolff, 1968; Smith and Snyder, 1979). The volume of this unit-cell is very close to half that of the 11-hydrate, which might indicate a novel polymorph of $MgSeO_4 \cdot 11H_2O$ with Z = 1 and, necessarily, space-group $P1$. Tick marks corresponding with this unit cell are shown in Figure 1.

C. Novel $MgSeO_4$ 9-hydrate

In contrast with the unknown hydrate described in the previous section the powder pattern observed from the quenched spherules was confidently indexed using DICVOL06 with a monoclinic unit cell: a = 7.271(1) Å, b = 10.509(1) Å, c = 17.408(2) Å, β = 109.46(1)°, and V = 1254.15 Å^3, the figures of merit being M(15) = 108.5 and F(15) = 237.3 (0.0023, 27). Additionally, systematic absences were identified that limited the likely space-groups to $P2_1$, Pc or $P2_1/c$.

Since it was highly likely that this phase was a magnesium selenate hydrate with general formula $MgSeO_4 \cdot nH_2O$, the problem was then to quantify n. In the absence of single crystals, the specimens being mixtures of an unknown hydrate and water ice, it is not possible to determine the hydration state using thermogravimetric methods. The unit-cell volumes of crystals with the formula $MgSeO_4 \cdot nH_2O$ and n = 0, 2, 4, 4½, 5, and 6 have been reported previously (Snyman & Pistorius, 1964: Stoilova & Koleva, 1995b: Kolitsch, 2002: Krivovichev, 2007); those with n = 7 and 11 have been determined in this and related work (Fortes & Gutmann, 2014). As shown in Figure 2, there is a near linear relationship between the hydration number, n, and the volume per formula unit. The problem now reduces to one of identifying a sensible combination of n and Z that falls on or around this line. The most plausible solution, shown by a red box in Figure 2, has n = 9 and Z = 4. Confidence in this determination is increased by noting that 9-hydrates have been found in quenched specimens of $MgSO_4$ and $MgCrO_4$ (although these have a different monoclinic unit-cell to that reported here and are presumably not isostructural), and also that Klein (1940) reported the occurrence of a $^9/_2$-hydrate, the structure of which was determined quite recently by Krivovichev (2007).

Perhaps the most convincing argument is the structure solution: the atomic structure was solved as $MgSeO_4 \cdot 9H_2O$ in space-group $P2_1/c$ from the X-ray powder diffraction data using the parallel tempering algorithm implemented in FOX, version 1.9.7.1 (Favre-Nicolin & Černý, 2002, 2004). FOX was initialised with the unit-cell parameters obtained by DICVOL06 and these were refined, along with peak profile coefficients, diffractometer zero-shift and background points by the LeBail method and by spline interpolation, respectively. Since ice Ih was present in the specimen, FOX was provided with crystallographic data for this phase (Fortes *et al.,* 2004), fitting these Bragg peaks by automatic adjustment of a simple scale factor. For the hydrate, FOX was used to construct ideal MgO_6 octahedra with Mg–O distances of 2.06 Å, and ideal SeO_4 tetrahedra with Se–O distances of 1.64 Å; these were treated as rigid bodies throughout the solution process. In ten runs of 1 million trials each, the crystal structure was optimized against the powder diffraction data, consistently producing very similar

structures with chemically sensible arrangements of the ionic polyhedra. Fourier difference maps phased on these structures revealed three peaks that seemed likely to correspond to the additional water molecules necessary to form a 9-hydrate. When FOX was re-run from scratch with three additional oxygen atoms included, the original structure was reproduced with the extra water oxygens being found in the same positions as the Fourier difference peaks. Ultimately the structure with the lowest overall cost function was exported as a CIF file to form the basis for Rietveld refinement with GSAS.

The sample temperature, −22°C, was used to obtain appropriate unit-cell parameters for the ice component in the specimen, from a linear interpolation of the values tabulated for H_2O ice Ih by Röttger *et al*. (1994). With the ice unit-cell parameters fixed, the specimen height and transparency (SHFT and TRNS parameters in GSAS peak shape function 3) were refined, these quantities being constrained to undergo equal shifts for both phases in the refinement. Sample scale, phase fraction, and six background coefficients were also refined, followed by the specimen unit-cell parameters and the Lorentzian 'microstrain' peak profile parameter, LY, and the peak asymmetry parameters S/L and H/L. A degree of preferred orientation in the ice component of the specimen was treated using a 6^{th}-order spherical harmonic model. Given the complexity of the structure, refinement of atomic coordinates was only done after a series of bond-distance and bond-angle restraints were entered; the values employed were intended to produce regular SeO_4 tetrahedra with Se–O bond lengths of 1.640 Å and regular MgO_6 octahedra with Mg–O bond lengths of 2.065 Å. These values are typical of other $MgSeO_4$-bearing crystals (e.g., Kolitsch *et al.,* 2002). After refinement to convergence of all atomic coordinates and of a common isotropic thermal displacement parameter for all heavy atoms, the locations of the hydrogen atoms were estimated geometrically. Examination of the first coordination shell of the water oxygens revealed a sensible pattern of O···O vectors consistent with hydrogen bonded contacts and so pairs of hydrogen atoms were sited at distances of 0.98 Å from each O atom along these vectors. With U_{iso} for all hydrogen atoms fixed, a further cycle of refinement was carried out, the final χ^2 value for the fit being 7.797, with weighted and unweighted profile R-factors (including the background) of 0.0640 and 0.0805

respectively. Table III reports the final structural parameters of $MgSeO_4 \cdot 9H_2O$: further details of this refinement are contained in a Crystallographic Information File included in the electronic supplement to this article; the reader may inspect the diffraction data using the freely available pdCIFplot software (Toby, 2003). The fit to the diffraction data is shown in Figure 3.

IV. DISCUSSION

The asymmetric unit of $MgSeO_4 \cdot 9H_2O$ is shown in Figure 4; bear in mind that the hydrogen atom positions (whilst chemically sensible) are estimated and not directly observed; these serve as predictions for any future neutron powder diffraction or single crystal diffraction study. Selected interatomic distances are listed in Tables IV and V. Despite the fairly light bond-distance restraints, some significant differences have emerged in the Mg–O lengths that are explicable in terms of the coordination of these water molecules. The water molecule with the longest Mg–O distance (Ow6) is the only one of the six Mg-coordinated waters to *accept* a hydrogen bond (from Ow9). A similar situation occurs in both $MgSO_4 \cdot 7H_2O$ and $MgSeO_4 \cdot 7H_2O$, where two of the Mg-coordinated waters accept a hydrogen bond each; these tetrahedrally coordinated waters exhibit Mg–O bond lengths of ~ 2.10 Å compared with ~ 2.05 Å for the other trigonally coordinated waters (Baur, 1964: Ferraris *et al.,* 1973: Fortes & Gutmann, 2014).

The packing of the polyhedral ions and neutral water molecules to form the complete structure is shown perpendicular to the *a*-axis in Figure 5, the inferred hydrogen bonding being depicted by dashed rods. A less cluttered schematic of the hydrogen bonding is shown in Figure 6, highlighting several salient features. Firstly, three of the Mg-coordinated waters, Ow1, Ow3 and Ow4, engage in H-bonding solely with the selenate oxygens: secondly, all but one of the selenate oxygens accepts three H-bonds, whereas O1 only accepts two H-bonds: thirdly, the interstitial water molecules prefer to both donate and accept hydrogen bonds from/to the Mg-coordinated waters and the selenate oxygens, there is only a

single H-bond between the Ow7 and Ow8 interstitial waters. None of these features are unusual, being observed also in $MgSO_4 \cdot 11H_2O$ (see H-bond scheme in Fortes *et al*., 2008); indeed, between the five interstitial waters of the 11-hydrate there is only one H-bond, the rest being between the Mg-coordinated waters and the sulfate oxygens. In other words, confidence in the structure solution (and the inferred network of hydrogen bonding) is strengthened by the occurrence of these architectural similarities.

The O···O distances (Table V) are, with one exception, tightly clustered around 2.8 Å (range 2.73 – 2.86 Å), which is the expected value for medium strength hydrogen-bonded contacts. The unusually long contact (Ow9 – Ow6) forms part of a rather interesting structural element, specifically a square ring or water tetramer (Figure 7). A similar four-sided ring of water molecules occurs in $Na_2SO_4 \cdot 10H_2O$; orientational disorder in this ring leads to significant differences in the anisotropic thermal expansion of $Na_2SO_4 \cdot 10H_2O$ depending on whether this disorder is frozen in by rapid cooling or whether an ordered state is achieved by slow cooling (*cf*., Brand *et al.,* 2009). With the current data I cannot rule out the possibility that the water molecules comprising the square ring in $MgSeO_4 \cdot 9H_2O$ are orientationally disordered. Future study of the material's thermal expansion and efforts to characterize the structure by single crystal methods must be used in order to establish this.

V. CONCLUSION

This work reports the discovery of at least two and possibly three new hydrates of $MgSeO_4$ formed by quenching of aqueous solutions in liquid nitrogen and subsequent rapid annealing of the resultant selenate-rich glass. One of these is an undecahydrate that is apparently isostructural with the sulfate analogue, $MgSO_4 \cdot 11H_2O$, but with an anisotropically strained unit-cell approximately 4 % larger in volume than the sulfate. The second new phase is an enneahydrate, $MgSeO_4 \cdot 9H_2O$; the heavy-atom structure of this compound has been determined from the X-ray powder diffraction data. The third phase appears to be a transient metastable hydrate that rapidly transforms to the more familiar 11-hydrate

structure. This may be a low-temperature polymorph of the 11-hydrate but further work is necessary to characterise it better.

The stability of the 9- and 11-hydrates with respect to one another and to the previously known heptahydrate remain to be confirmed. Upon warming, the 11-hydrate has been found to transform (presumably by incongruent melting) to the 9-hydrate. Conversely, crystals of $MgSeO_4 \cdot 7H_2O$ stored in a freezer at −20 °C for two weeks were discovered to have transformed, both to the intrigue and irritation of the author, entirely to the 9-hydrate. This rather suggests that the 9-hydrate is the stable phase at low temperature and that a re-evaluation of the binary phase diagram is in order.

ACKNOWLEDGEMENT

ADF acknowledges financial support from the Science and Technology Facilities Council, grant numbers PP/E006515/1 and ST/K000934/1.

References

Baur, W. H. (**1964**). "On the crystal chemistry of salt hydrates. IV. The refinement of the crystal structure of $MgSO_4 \cdot 7H_2O$ (epsomite)," Acta Crystallogr. **17**, 1361-1369.

Boultif, A., and Louër, D. (**2004**). "Powder pattern indexing with the dichotomy method," J. Appl. Cryst. **37**, 724-731.

Brand, H. E. A., Fortes, A. D., Wood, I. G., Knight, K. S., and Večadlo, L. (**2009**). "The thermal expansion and crystal structure of mirabilite ($Na_2SO_4 \cdot 10D_2O$) from 4.2 – 300 K, determined by time-of-flight neutron powder diffraction," Phys. Chem. Min. **36**, 29-46.

De Wolff, P. M. (**1968**). "A simplified criterion for the reliability of a powder pattern indexing," J. Appl. Cryst. **5**, 108-113.

Favre-Nicolin, V., and Černý, R. (**2002**). "FOX, 'free objects for crystallography': a modular approach to *ab initio* structure determination from powder diffraction," J. Appl. Cryst. **35**, 734-743.

Favre-Nicolin, V., and Černý, R. (**2004**). "A better FOX: using flexible modeling and maximum likelihood to improve direct-space *ab initio* structure determination from powder diffraction," Z. Krist. **219**, 847-856.

Ferraris, G., Jones, D. W., and Yerkess, J. (**1973**). "Refinement of the crystal structure of magnesium sulphate heptahydrate (epsomite) by neutron diffraction," J. Chem. Soc. Dalton Trans. **1973**, 816-821.

Fortes, A. D. (**2014**). "Analogue materials for high-pressure studies of planetary ices," British Crystallographic Society Spring Meeting, Loughborough, April 8th 2014.

Fortes, A. D., and Gutmann, M. J. (**2014**). "Crystal structure of magnesium selenate heptahydrate, $MgSeO_4 \cdot 7H_2O$, from neutron time-of-flight data," Acta Crystallogr. Sect. E. **70**, 134-137.

Fortes, A. D., and Wood, I. G. (**2012**). "X-ray powder diffraction analysis of a new magnesium chromate hydrate, $MgCrO_4 \cdot 11H_2O$," Powder Diffr. **27**, 8-11.

Fortes, A. D., Browning, F., and Wood, I. G. (**2012a**). "Cation substitution in synthetic meridianiite ($MgSO_4 \cdot 11H_2O$) I: X-ray powder diffraction analysis of quenched polycrystalline aggregates," Phys. Chem. Min. **39**, 419-441.

Fortes, A. D., Browning, F., and Wood, I. G. (**2012b**). "Cation substitution in synthetic meridianiite ($MgSO_4 \cdot 11H_2O$) II: Variation in unit-cell parameters determined from X-ray powder diffraction data," Phys. Chem. Min. **39**, 443-454.

Fortes, A. D., Wood, I. G., and Fernandez-Alonso, F. (**2012c**). "Thermoelastic properties and high-pressure decomposition of $MgSO_4 \cdot 11D_2O$," ISIS Experimental Report, RB1110039, Rutherford Appleton Laboratory, Oxford, UK.

Fortes, A. D., Wood, I. G., and Gutmann, M. J. (**2013**). "$MgSO_4 \cdot 11H_2O$ and $MgCrO_4 \cdot 11H_2O$ from time-of-flight neutron single-crystal Laue data," Acta Crystallogr. Sect. C **69**, 324-329.

Fortes, A. D., Wood, I. G., and Knight, K. S. (**2008**). "The crystal structure and thermal expansion tensor of $MgSO_4 \cdot 11D_2O$ (meridianiite) determined by neutron powder diffraction," Phys. Chem. Min. **35**, 207-221.

Fortes, A. D., Wood, I. G., and Tucker, M. G. (**2009**). "The effect of pressure on the structure of meridianiite ($MgSO_4 \cdot 11D_2O$)," ISIS Experimental Report, RB910226, Rutherford Appleton Laboratory, Oxford, UK.

Fortes, A. D., Wood, I. G., Grigoriev, D., Alfredsson, M., Kipfstuhl, S., Knight, K. S., and Smith, R. I. (**2004**). "No evidence of large-scale proton ordering in Antarctic ice from powder neutron diffraction," J. Chem. Phys. **120**, 11376-11379.

Genceli, F. E., Shinochirou, H., Yoshinori, I., Toshimitsu, S., Hondoh, T., Kawamura, T., and Witkamp, G. –J. (**2009**). "Meridianiite detected in ice," J. Glaciol. **55**, 117-122.

Kamburov, S., Schmidt, H., Voigt, W., and Balarew, C. (**2014**). "Similarities and peculiarities between the crystal structures of the hydrates of sodium sulfate and selenate," Acta Crystallogr. Sect. B **70**, 714-722.

Kargel, J. S. (**1991**). "Brine volcanism and the interior structures of asteroids and icy satellites," Icarus **94**, 368-390.

Klein, A. (**1940**). "Étude sur les séléniates des métaux de la série magnésienne," Ann. Chim. **14**, 263-317.

Kolitsch, U. (**2001**). "Copper(II) selenate pentahydrate, $CuSeO_4 \cdot 5H_2O$," Acta Crystallogr. Sect. E **57**, i104-i105.

Kolitsch, U. (**2002**). "Magnesium selenate hexahydrate, $MgSeO_4 \cdot 6H_2O$," Acta Crystallogr., Sect. E **58**, i3-i5.

Krivovichev, S. V. (**2007**). "Crystal chemistry of selenates with mineral-like structures. III. Heteropolyhedral chains in the crystal structure of $[Mg(H_2O)_4(SeO_4)]_2(H_2O)$," Geol. Ore Dep. **49**(7), 537-541.

Larson, A. C., and Von Dreele, R. B. (2000). *General Structure Analysis System (GSAS)*. Los Alamos National Laboratory Report, LAUR 86-748.

Meyer, J., and Aulich, W. (**1928**). "Zur kenntnis der doppelsalze der selensäure," Z. Anorg. Allg. Chem. **172**, 321-343.

Peterson, R. C. and Wang, R. (**2006**). "Crystal molds on Mars: melting of a possible new mineral species to create Martian chaotic terrain," Geology **34**, 957-960.

Peterson, R. C., Nelson, W., Madu, B., and Shurvell, H. F. (**2007**). "Meridianiite: a new mineral species observed on Earth and predicted to exist on Mars," Am. Min. **92**, 1756-1759.

Putz, H., and Brandenburg, K. (**2006**). *Diamond - Crystal and Molecular Structure Visualization*. Crystal Impact - GbR, Kreuzherrenstr. 102, 53227 Bonn, Germany. http://www.crystalimpact.com/diamond

Röttger, K., Endriss, A., Ihringer, J., Doyle, S., and Kuhs, W. F. (**1994**). "Lattice constants and thermal expansion of H_2O and D_2O ice Ih between 10 and 265 K," Acta Crystallogr., Sect. B **50**, 644-648.

Smith, G. S., and Snyder, R. L. (**1979**). "F_N: a criterion for rating powder diffraction patterns and evaluating the reliability of powder-pattern indexing," J. Appl. Cryst. **12**, 60-65.

Stoilova, D., and Koleva, V. (**1995a**). "Thermal dehydration of magnesium selenate hydrates," Thermochim. Acta **255**, 33-38.

Stoilova, D., and Koleva, V. (**1995b**). "X-ray diffraction study on $MgSeO_4 \cdot 6H_2O$ at elevated temperatures," Cryst. Res. Tech. **30**, 547-551.

Toby, B. H. (**2001**). "*EXPGUI*, a graphical user interface for *GSAS*," J. Appl. Cryst. **34**, 210-213.

Toby, B. H. (**2003**). "CIF applications. XII. Inspecting Rietveld fits from pdCIF: *pdCIFplot*," J. Appl. Cryst. **36**, 1285-1287.

Weil, M., and Bonneau, B. (**2014**). "Crystal structures of $Na_2SeO_4 \cdot 1.5H_2O$ and $Na_2SeO_4 \cdot 10H_2O$," Acta Cryst. Sect. E **70**, 54-57.

Wood, I. G., Hughes, N., Browning, F., and Fortes, A. D. (**2012**). "A compact transportable, thermoelectrically-cooled cold stage for reflection geometry X-ray powder diffraction," J. Appl. Crystallogr. **45**, 608-610.

Table I

Comparison of the unit-cell parameters of the three isostructural oxyanion analogues $MgXO_4 \cdot 11H_2O$. Each of these were measured at approximately −22 °C and corrections for sample height were made using water ice as an internal standard using the unit-cell parameters as a function of temperature reported by Röttger *et al.* (1994).

	$MgSO_4 \cdot 11H_2O$ [a]	$MgCrO_4 \cdot 11H_2O$ [a]		$MgSeO_4 \cdot 11H_2O$ [b]	
		absolute	strain (%)	absolute	strain (%)
a (Å)	6.74895(13)	6.81133(8)	+0.92	6.77900(8)	+0.45
b (Å)	6.81768(13)	6.95839(9)	+2.06	6.96516(9)	+2.16
c (Å)	17.2993(3)	17.3850(2)	+0.50	17.4934(2)	+1.12
α (°)	88.118(2)	88.920(1)	−0.22	87.713(1)	−0.46
β (°)	89.467(2)	89.480(1)	+0.01	89.222(1)	−0.27
γ (°)	62.717(1)	62.772(1)	+0.10	63.121(1)	+0.64
V (Å^3)	707.00(2)	732.17(1)	+3.56	736.15(1)	+4.12

[a] Fortes & Wood (2012)
[b] This work (*cf.*, section III.A)

Table II

Refined atomic coordinates (*x,y,z*) and fixed isotropic displacement parameters (U_{iso}) for the heavy atoms in the meridianiite-structured $MgSeO_4 \cdot 11H_2O$ (*cf.*, Section III.A) compared to those obtained previously for meridianiite-structured $MgCrO_4 \cdot 11H_2O$ by neutron time-of-flight diffraction methods (Fortes & Wood, 2012). This X-ray powder refinement yielded Rp = 0.0845 and $\chi^2 = 2.897$ for 57 variables.

	$MgSeO_4 \cdot 11H_2O$				$MgCrO_4 \cdot 11H_2O$			
	x	*y*	*z*	U_{iso} (x100)	*x*	*y*	*z*	U_{iso} (x100)
Se / Cr	0.4022(7)	0.3279(8)	0.2011(3)	0.80	0.4070(7)	0.3184(8)	0.2026(3)	4.9(3)
O1	0.309(4)	0.333(3)	0.113(1)	0.80	0.2938(17)	0.3385(18)	0.1179(3)	1.3(1)
O2	0.202(3)	0.456(3)	0.270(1)	0.80	0.2117(13)	0.4441(14)	0.2650(4)	1.3(1)
O3	0.544(3)	0.066(3)	0.236(1)	0.80	0.5442(15)	0.0628(7)	0.2301(6)	1.3(1)
O4	0.594(3)	0.420(3)	0.193(1)	0.80	0.5768(15)	0.4260(15)	0.1998(7)	1.3(1)
Mg1	1.000	0.000	0.000	0.80	1.000	0.000	0.000	4.6(4)
Mg2	1.000	0.000	0.500	0.80	1.000	0.000	0.500	4.6(4)
Ow1	0.631(3)	0.190(3)	0.005(1)	0.80	0.6581(2)	0.1854(13)	0.0084(6)	1.3(1)
Ow2	0.977(3)	−0.257(3)	0.054(1)	0.80	0.9780(17)	-0.2619(10)	0.0546(5)	1.3(1)
Ow3	1.056(3)	0.106(3)	0.107(1)	0.80	1.0413(16)	0.1052(14)	0.1070(2)	1.3(1)
Ow4	1.145(3)	−0.096(3)	0.393(1)	0.80	1.1527(15)	-0.1051(14)	0.3942(3)	1.3(1)
Ow5	0.813(3)	−0.158(3)	0.483(1)	0.80	0.8180(14)	-0.1700(14)	0.4854(6)	1.3(1)
Ow6	0.742(3)	0.283(3)	0.448(1)	0.80	0.7498(11)	0.2725(9)	0.4445(5)	1.3(1)
Ow7	0.287(3)	0.419(3)	0.422(1)	0.80	0.3156(21)	0.4060(20)	0.4208(7)	1.3(1)
Ow8	0.593(3)	−0.233(3)	0.119(1)	0.80	0.6047(19)	-0.2391(20)	0.1159(6)	1.3(1)
Ow9	0.558(3)	−0.148(3)	0.362(1)	0.80	0.5562(19)	-0.1516(21)	0.3616(7)	1.3(1)
Ow10	0.822(3)	0.450(3)	0.314(1)	0.80	0.8311(20)	0.4439(20)	0.3136(7)	1.3(1)
Ow11	1.003(3)	−0.096(3)	0.246(1)	0.80	1.0005(20)	-0.0975(20)	0.2473(6)	1.3(1)

Table III

Refined atomic coordinates (*x,y,z*) and isotropic displacement parameters (U_{iso}) for the heavy atoms in $MgSeO_4 \cdot 9H_2O$ along with hydrogen atom locations estimated on the basis of the observed coordination geometry of neighbouring water oxygens. See also the supplementary CIF data.

	x	*y*	*z*	U_{iso} (x100)
Se	0.6075(2)	0.4413(1)	0.3327(1)	0.80(4)
O1	0.6640(10)	0.2931(3)	0.3215(4)	0.80(4)
O2	0.3775(5)	0.4529(7)	0.3270(4)	0.80(4)
O3	0.6419(10)	0.5347(6)	0.2629(4)	0.80(4)
O4	0.7484(9)	0.4906(6)	0.4228(3)	0.80(4)
Mg	0.8988(6)	0.2953(4)	0.1237(2)	0.80(4)
Ow1	1.1565(8)	0.2647(7)	0.2186(4)	0.80(4)
Ow2	1.0435(10)	0.3833(6)	0.0544(4)	0.80(4)
Ow3	0.9185(10)	0.1200(5)	0.0735(4)	0.80(4)
Ow4	0.7303(10)	0.2095(6)	0.1835(4)	0.80(4)
Ow5	0.8946(11)	0.4727(5)	0.1754(4)	0.80(4)
Ow6	0.6430(8)	0.3301(6)	0.0275(4)	0.80(4)
Ow7	0.9815(10)	0.6832(6)	0.1024(4)	0.80(4)
Ow8	0.6581(10)	0.8394(7)	0.0336(4)	0.80(4)
Ow9	0.4038(10)	0.5029(6)	0.0988(4)	0.80(4)
H1a	*1.227*	*0.184*	*0.225*	*3.0*
H1b	*1.234*	*0.330*	*0.256*	*3.0*
H2a	*1.035*	*0.360*	*−0.001*	*3.0*
H2b	*1.171*	*0.426*	*0.070*	*3.0*
H3a	*0.858*	*0.081*	*0.020*	*3.0*
H3b	*1.037*	*0.074*	*0.075*	*3.0*
H4a	*0.707*	*0.240*	*0.233*	*3.0*
H4b	*0.692*	*0.120*	*0.180*	*3.0*
H5a	*0.807*	*0494*	*0.206*	*3.0*
H5b	*0.926*	*0.548*	*0.149*	*3.0*
H6a	*0.536*	*0.269*	*0.006*	*3.0*
H6b	*0.627*	*0.389*	*−0.018*	*3.0*
H7a	*1.109*	*0.723*	*0.130*	*3.0*
H7b	*0.868*	*0.738*	*0.079*	*3.0*
H8a	*0.645*	*0.879*	*0.083*	*3.0*
H8b	*0.688*	*0.898*	*−0.004*	*3.0*
H9a	*0.487*	*0.514*	*0.156*	*3.0*
H9b	*0.481*	*0.448*	*0.076*	*3.0*

Table IV

Bond lengths in the polyhedral ions of $MgSeO_4 \cdot 9H_2O$

Bond	Length (Å)	Bond	Length (Å)
Se–O1	1.639(3)	Mg–Ow1	2.069(4)
Se–O2	1.646(3)	Mg–Ow2	2.064(4)
Se–O3	1.645(3)	Mg–Ow3	2.065(4)
Se–O4	1.645(3)	Mg–Ow4	2.061(4)
		Mg–Ow5	2.075(4)
		Mg–Ow6	2.079(4)

Table V

O···O bond lengths in $MgSeO_4 \cdot 9H_2O$. Roman numeral superscripts indicate the symmetry codes listed underneath the table.

H-bonded contact	Length (Å)	H-bonded contact	Length (Å)
Ow1···O3 (i)	2.79(1)	Ow5···Ow7	2.73(1)
Ow1···O2 (ii)	2.83(1)	Ow6···Ow8 (vi)	2.75(1)
Ow2···Ow7 (iii)	2.76(1)	Ow6···Ow9 (vi)	2.74(1)
Ow2···Ow9 (ii)	2.77(1)	Ow7···O1 (vii)	2.73(1)
Ow3···O4 (iv)	2.76(1)	Ow7···Ow8	2.79(1)
Ow3···O4 (i)	2.76(1)	Ow8···O2 (viii)	2.79(1)
Ow4···O1	2.75(1)	Ow8···O4 (ix)	2.86(1)
Ow4···O2 (v)	2.80(1)	Ow9···O3	2.82(1)
Ow5···O3	2.83(1)	Ow9···Ow6	3.05(1)

(i) = 2−*x*, −0,5+*y*, 0.5−*z*: (ii) = 1+*x*, *y*, *z*: (iii) = 2−*x*, 1−*y*, −*z*: (iv) = *x*, 0.5−*y*, −0.5+*z*: (v) = 1−*x*, −0.5+*y*, 0.5−*z*: (vi) = 1−*x*, 1−*y*, −*z*: (vii) = 2−*x*, 0.5+*y*, 0.5−*z*: (viii) = 1−*x*, 0.5+*y*, 0.5−*z*: (ix) = *x*, 1.5−*y*, −0.5+*z*.

Figure 1

(Colour online) Representative X-ray powder diffraction patterns of the three $MgSeO_4$ hydrates observed during this study (see section III for discussion).

Figure 2

(Colour online) Relationship between hydration number, *n*, and volume per formula unit amongst the known $MgSeO_4$ hydrates (filled diamonds) and the proposed new 9-hydrate (open square). Based on data in Snyman & Pistorius (1964), Stoilova & Koleva (1995b), Kolitsch (2002), Krivovichev (2007), Fortes & Gutmann (2014) and this work.

Figure 3

(Colour online) X-ray powder diffraction pattern of $MgSeO_4 \cdot 9H_2O$ fitted to the newly-obtained structure by the Rietveld method. Red circles represent the measured data, the green line is the fit to the data and the purple line underneath the powder pattern is the difference profile. Tick marks show the expected positions of Bragg peaks from the 9-hydrate (upper set) and ice Ih (lower set). The inset depicts a magnified view of the low-2θ range.

Figure 4

(Colour online) The asymmetric unit of $MgSeO_4 \cdot 9H_2O$. Drawn using Diamond (Putz & Brandenburg, 2006). Note that the positions of the hydrogen atoms are inferred on the basis of oxygen coordination geometry and interatomic vectors and are not directly determined from the X-ray powder data.

Figure 5

(Colour online) Unit cell of $MgSeO_4 \cdot 9H_2O$ viewed parallel to the *a*-axis (i.e., towards the *b*–*c* plane) showing the relative arrangement of the $Mg(H_2O)_6$ octahedra (green) and the SeO_4 tetrahedra (purple). The inferred hydrogen bond framework is illustrated with dashed rods.

Figure 6

(Colour online) Cartoon illustration of the inferred hydrogen bond scheme in $MgSeO_4 \cdot 9H_2O$.

Figure 7

(Colour online) The square ring of hydrogen-bonded water molecules involving Ow6 and Ow9 in relation to one of the 2_1 screw axes. Note that H6a lies out of the plane of the square ring in front of (top left) and behind (bottom right) Ow6.

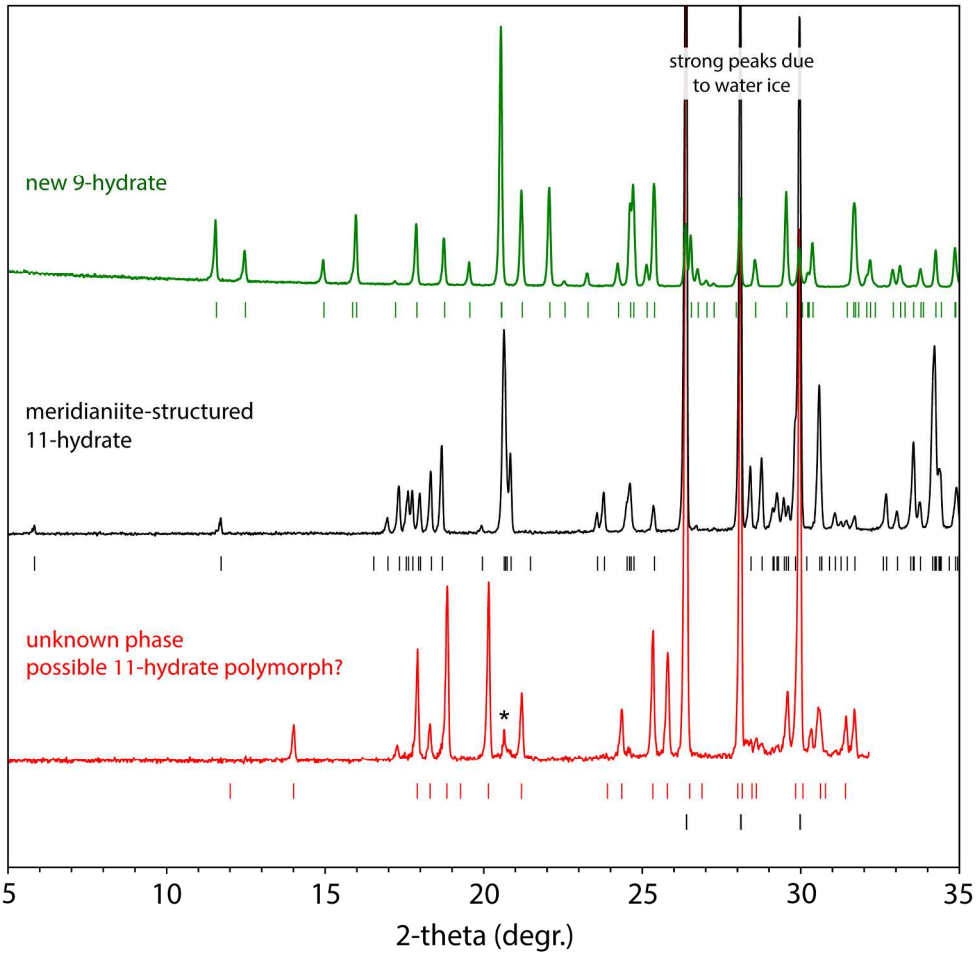

209x203mm (300 x 300 DPI)

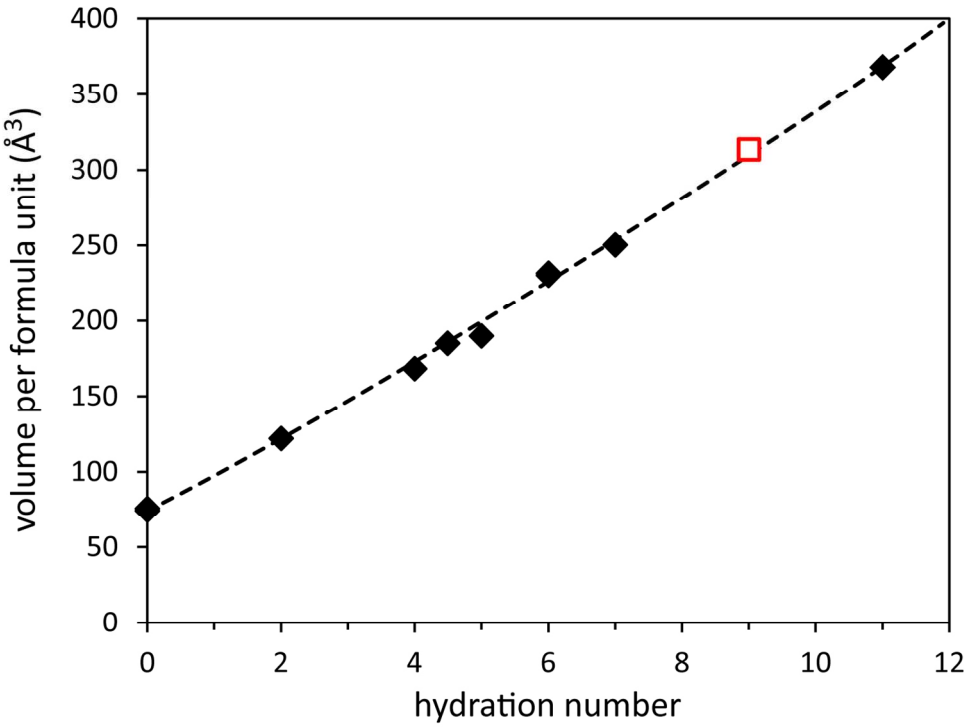

135x100mm (300 x 300 DPI)

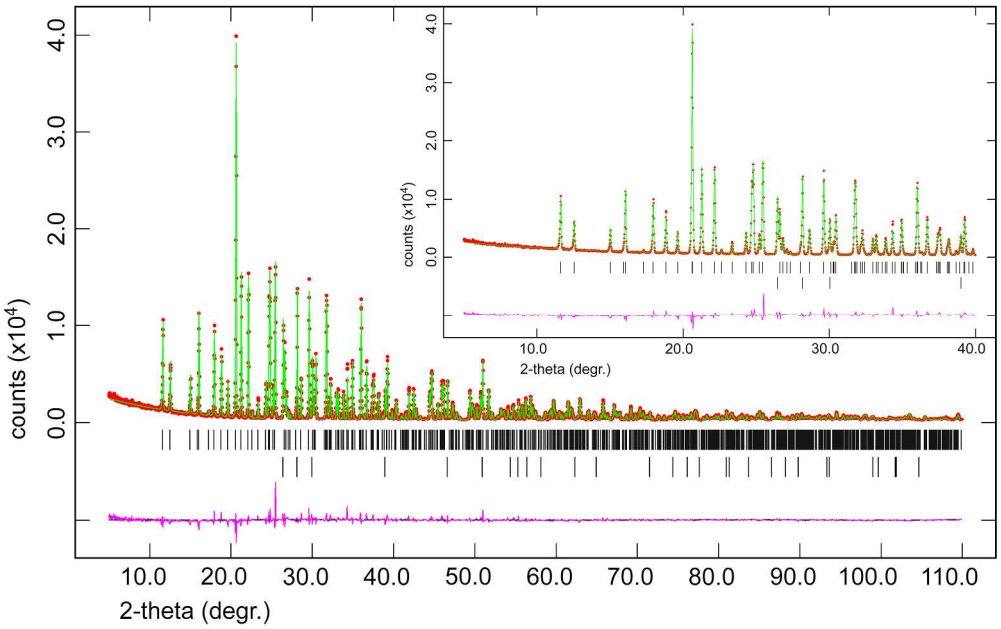

338x212mm (300 x 300 DPI)

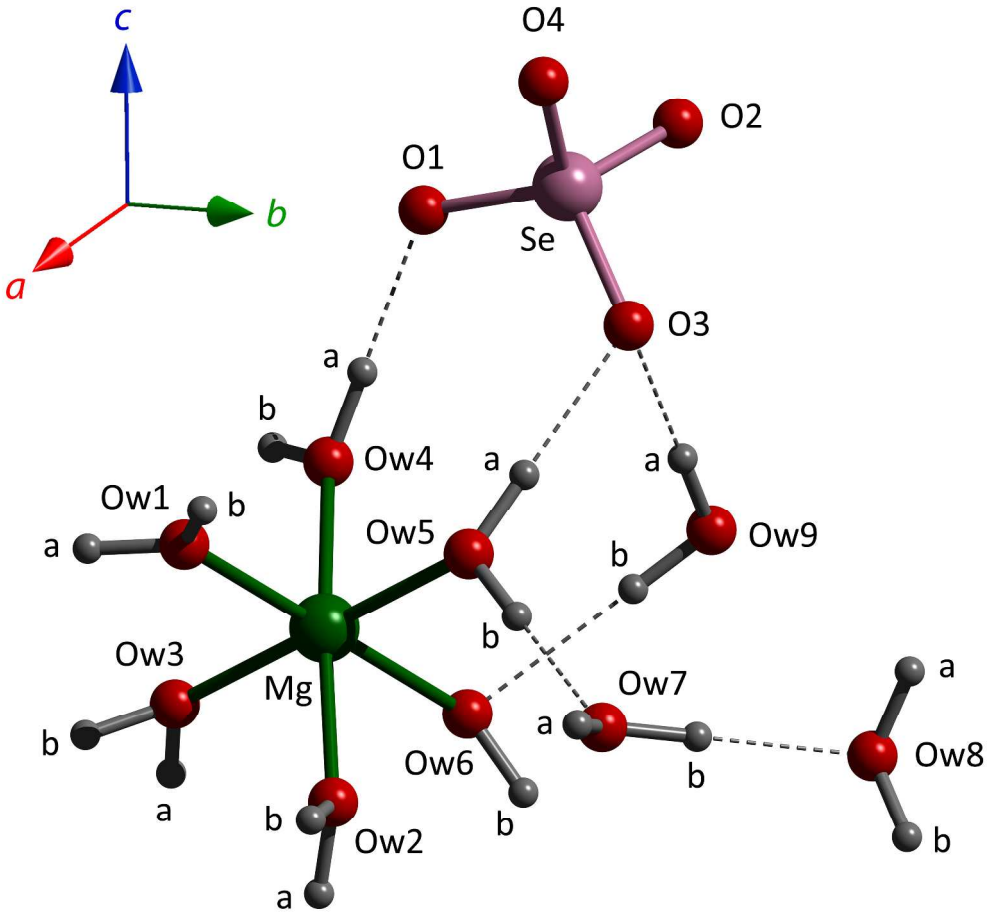

313x289mm (300 x 300 DPI)

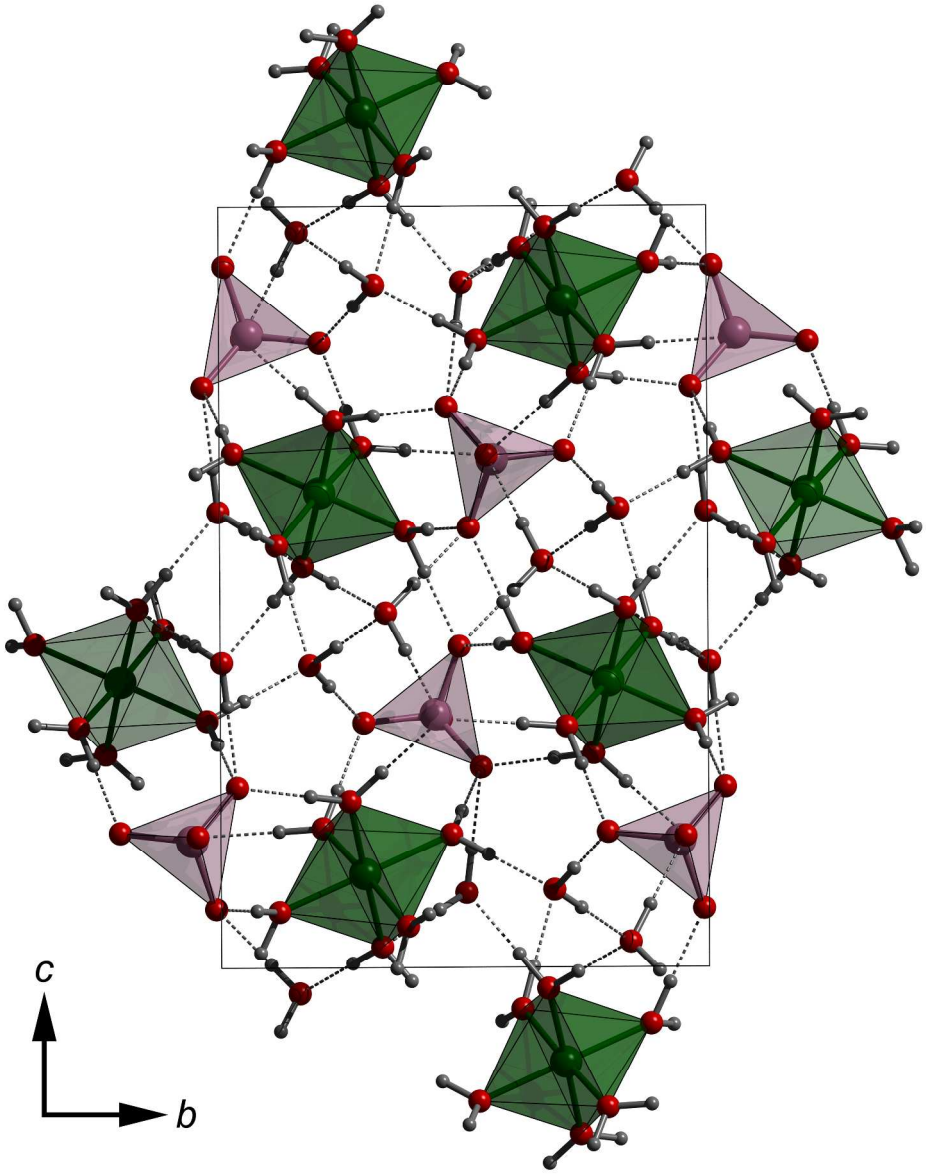

296x362mm (300 x 300 DPI)

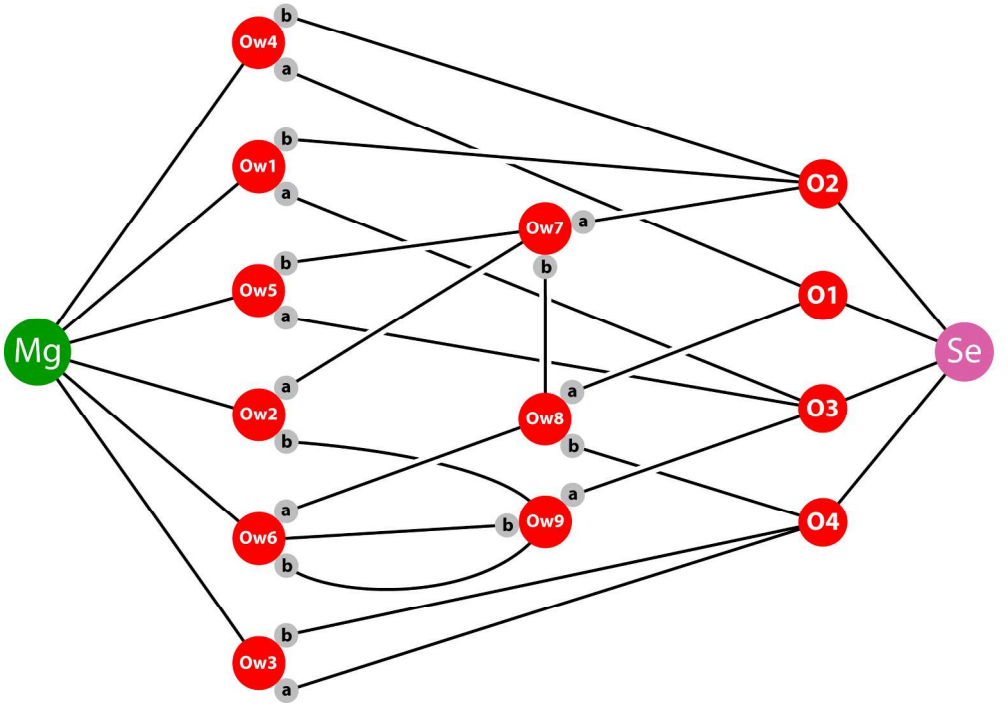

213x163mm (300 x 300 DPI)

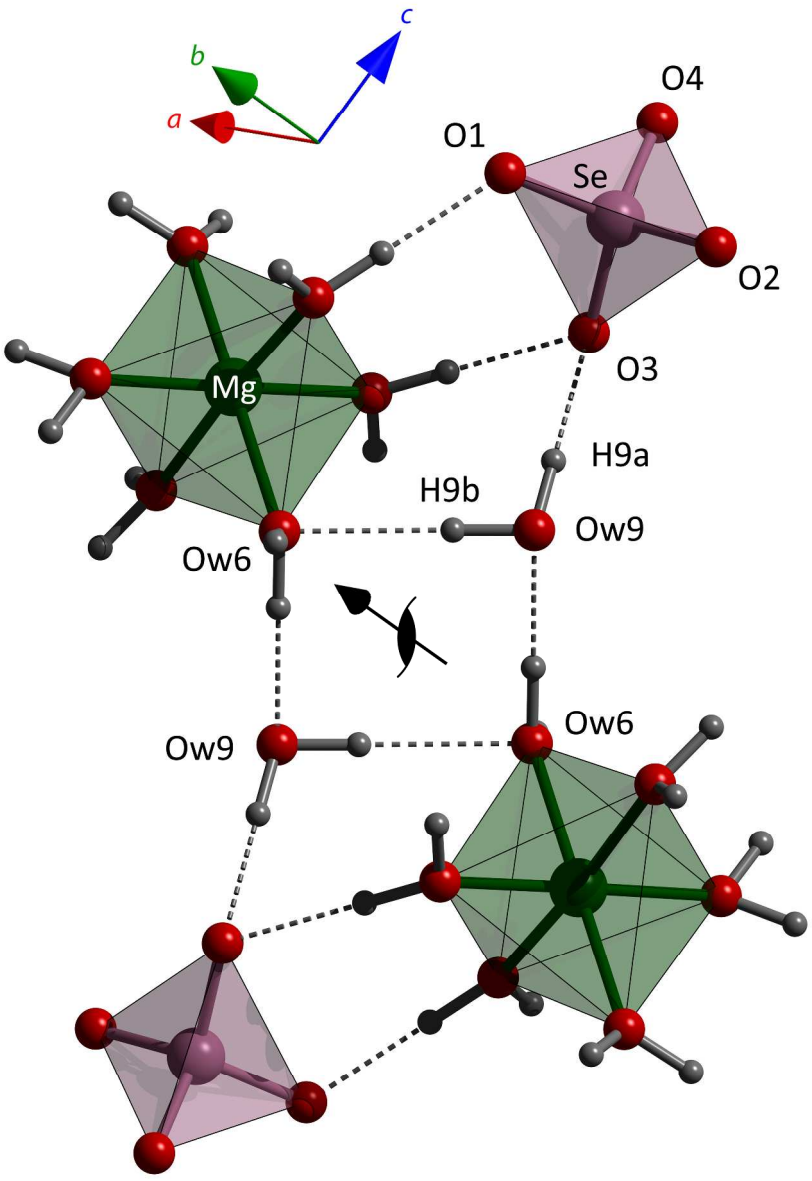

296x423mm (300 x 300 DPI)